quaternary

MDPI

Article

Holocene coastal evolution of the eastern Iranian Makran: Insights on seismic activity based on beach morphology and sedimentology

Raphaël Normand[1*], Guy Simpson[1], Frédéric Herman[2], Rabiul Haque Biswas[2] & Abbas Bahroudi[3]

[1] Department of Earth Sciences, University of Geneva, Rue des Maraîchers 13, 1205 Geneva, Switzerland. Raphael.normand@unige.ch, guy.simpson@unige.ch

[2] Institute of Earth Surface Dynamics, Faculty of Geosciences and Environment, University of Lausanne, 1012 Lausanne, Switzerland. Frederic.herman@unil.ch, rabiulhaque.biswas@unil.ch

[3] Exploration department, School of Mining Engineering, University of Tehran, Northern Kargar avn, P.O. Box 11365-4563, Tehran. Bahroudi@ut.ac.ir

* Correspondence: raphnormand@gmail.com

Academic Editor: name

Received: date; Accepted: date; Published: date

Abstract: The Makran coast displays evidence of surface uplift since at least the Late Pleistocene, but it remains uncertain whether this displacement is accommodated by creep on the subduction interface, or in a series of large earthquakes. Here, we address this problem by looking at the short term (Holocene) history of continental vertical displacements recorded in the geomorphology and sedimentary succession of the Makran beaches. In the region of Chabahar (Southern Iran), we study two bay-beaches through the description, measurement and dating of 13 sedimentary sections with a combination of radiocarbon and Optically Stimulated Luminescence (OSL) dating. Our results show that lagoonal settings dominate the early Holocene. A flooding surface associated with the Holocene maximum transgression is followed by a prograding sequence of tidal and beach deposits. In Pozm bay, we observe a rapid horizontal progradation of the beach ridge succession (3.5 m/y over the last 1950 years). A 3150 year old flooding surface within the sedimentary succession of Chabahar bay is interpreted as a coseismic subsidence event. Although the western Makran subduction zone has been aseismic for several centuries, the coastal geological record reveals the occurrence of a sudden vertical displacement and complex uplift patterns, which in the context of a subduction zone could reasonably be attributed to the occurrence of ancient earthquakes.

Keywords: Makran, coastal processes, coseismic subsidence, Holocene uplift, headland-bay beach, beach progradation

1. Introduction

The Makran coast, in southeastern Iran, sits above oceanic lithosphere of the Arabian plate that is currently subducting northward under Eurasia. The coast has clearly experienced long-term uplift throughout the Late Pleistocene, as evidenced by the presence of emerged sequences of marine terraces, some of which outcrop at more than a hundred meters above present sea-level [1–3]. In the eastern Makran (Pakistan), surface uplift of the coastal margin appears to be closely linked with large earthquakes, the last of which was a Mw 8.1 thrust event in 1945 [4,5]. However, in the western segment of the Makran (Iran), there is no obvious historical evidence for large earthquakes in the last 1000 years [6–9]. It is currently unclear whether the lack of seismicity reflects a different mechanical behavior at the subduction interface, or if infrequent large earthquakes occurred in the past and should be expected to happen again [10–12]. Here, we studied Holocene beach deposits to try to better understand the nature of vertical motions in the Makran over the last 10'000 years.

Due to their close relation to mean sea level, beaches are prone to record relative sea-level changes related to coseismic vertical motions, as commonly observed in subduction zones [13,14]. Along a coastline experiencing coseismic uplift, a beach staircase profile can develop due to the sudden abandonment of the active ridge during earthquakes [15]. Inversely, in regions experiencing coseismic subsidence, remobilization of the sediments from the destroyed frontal part of the beach into a new active beach ridge situated further seaward has been observed to happen in the few years following earthquakes [16]. On the other hand, if the western Makran is behaving aseismically, the deformation is accommodated on long time scales and there should be no signs of perturbation in the beaches.

Although several studies have considered the long-term uplift recorded by the spectacular Pleistocene marine terraces exposed along the Makran coast [5,17–19], relatively little attention has been focused on the shorter-term record. Paleoseismic studies from the Makran coastline have mainly focused on the tsunami risk associated with megathrust earthquakes within the MSZ [20,21,8,22–25]. A few studies have published palesoseismic evidences associated with the Mw 8.1 1945 eastern Makran earthquake [26,10], but geological evidences for older events have rarely been described [27]. Studies focusing on the beach ridge succession of Chabahar bay have not considered the potential for coseismic vertical motion [28–30].

In this study, we have analyzed the development of two bay-beaches of the Iranian Makran; Chabahar bay and Beris bay (Fig. 1). We measured 11 and 2 sections respectively in these bays in order to understand the history of the beaches using the sedimentary succession of recent deposits. To add time constrains, we sampled relevant intervals for both radiocarbon and optically stimulated luminescence dating (OSL). Furthermore, we visited and sampled the beach ridge succession of Pozm bay in order to get insights on coastal progradation. Fluvial sedimentary input was assessed through a study of the watersheds of main tributaries. Our results shed light on the landscape evolution of the region over the Holocene, driven by the interaction between sediment input, eustatic sea level variation and vertical tectonic motion.

2. Geological setting

The Makran subduction zone (MSZ) is the result of northwards subduction of the Arabian plate under Eurasia [4,31,32,10,8]. Although the margin is currently active, as indicated by GPS [33–35] and recently uplifted marine terraces [5,18,36,19,2], seismic activity of the Makran remains relatively low compared to other subduction zones. The eastern segment has experienced several thrust earthquakes, notably the Mw 8.1 in 1945 [4] and a recent Mw 6.3 event in 2017 [12]. However, the western segment (the focus of this study) has seemingly not experienced any thrust earthquake since the historical events of 1008 or 1483 [6,8], whose exact magnitudes, epicenter positions and focal mechanisms remain controversial [9].

The bedrock geology at the coastal plain [37,38,5,39–41,2,1,42,43] is dominated by erodible Tertiary marl forming the flat coastal strip (Fig. 1). The coastal plain is occasionally punctuated by prominent headlands, whose bedrock geology is dominated by more resistant, late tertiary calcareous sandstones.

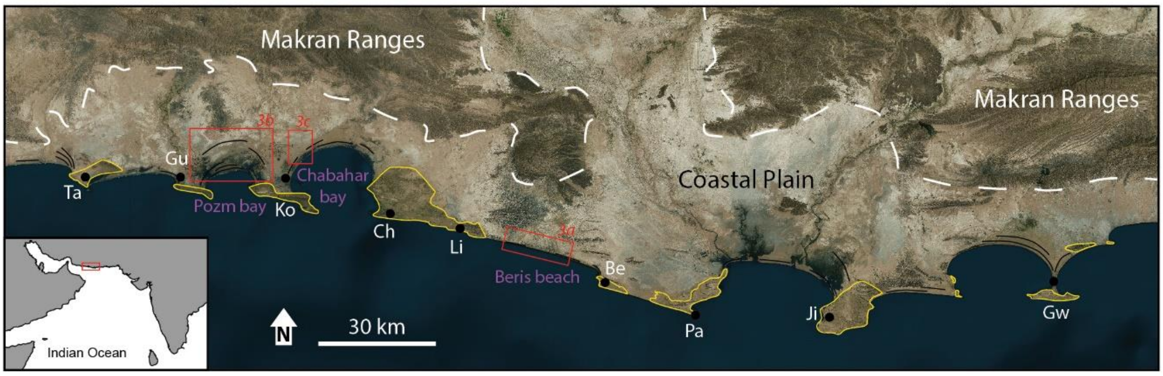

Figure 1. General satellite view of a segment of the Makran coast (image Bing satellite). White dashed line : rough delineation of the Makran ranges. Black lines : beach ridges. Yellow outlines : protruding headlands. Purple names: studied regions. Red squares: position of Figures 3a, 3b and 3c. Ta : Tang, Gu : Gurdim, Ko : Konarak, Ch : Chabahar, Li : Lipar, Be : Beris, Ji : Jiwani, Gw : Gwadar.

The climate in Makran is arid to semi-arid and has been so for at least 5000 years [44–46]. This makes it possible to interpret the Holocene depositional record based on the current coastal setting. The mean annual precipitation is low (127 mm), and occurs mostly during winter [47,48]. Rivers are dry most of the year, but activate during heavy rain episodes resulting in flash flood events inundating the coastal plain and bringing large amounts of sediments to the sea [2,47,1,39,49]. The tide range is micro to mesotidal (1.8-3m) [18,28], and the current wave regime in Chabahar is mostly towards the NNW, with a maximum significant wave height of 3 m [50,28]. Based on a record spanning 1985-2007, winds come mostly from the south and the west [50,51].

Only a few previous studies have focused on the Holocene coastal depositional record of the Makran. Radiocarbon dating indicate that they have been developing since the mid-Holocene highstand, around 6000 BP [47,29,30,2,10,48,5,28,52] (supplementary table S1.1). Some authors have argued on the strong mobility of the coastal region during the Holocene, as the coastline seem to have advanced by up to 20 km since the mid-Holocene maximum transgression [47,53]. Moreover, it has been proposed that the Gurdim and Konarak headlands used to be islands that were progressively attached to the mainland by widening tombolos, evolving into the current omega shaped bay morphology (Fig. 1) [2,18,49,29]. The Chabahar bay-beach has been shown to prograde at about 0.7 m/yr between 5438 and 1200 BP, reducing to 0.12 m/yr since then [29]. However, dating results from a recent study of the same strandplain imply a much more continuous progradation of 1-2.2 m/yr (faster for younger samples) [28].

Signs of the presence of lagoonal systems during the mid-Holocene highstand in the coastal Pakistani Makran has been observed [47,53]. Some of these ancient lagoons have evolved to low-lying flats, such as those observable west of Pasni and northwest of Gwadar, due to their complete filling by fine alluvial sediments. In fact, we can currently observe that the large active lagoons of the Makran, such as that of Kalat or Miani (Pakistan), host river deltas and will one day be entirely filled.

3. Methods

3.1 Fieldwork

Our approach to study the past and present history of the Makran Holocene beaches was to search for natural transects, where beach sedimentary successions could be observed. We visited, logged and sampled two localities. The first transect, where we measured two logs (facies 1 to 6, logs B1 and B2), is a 400m long natural river cut through the longshore beach between Beris village and Lipar lake (hereafter referred to as "Beris beach") (Fig. 1). The second transect, where we measured eleven logs (facies A to G, logs K1 to K11), is a 4.5 km long man-made trench through the coastal plain near Konarak airport, within Chabahar bay (Fig. 1). We studied the successions by describing the different facies encountered and their spatial (lateral) and chronological (vertical) relation with each other. Ultimately, we try to interpret these facies in terms of depositional setting, with the help of observations made on the current Makran coastal depositional system, in order to have an idea of the Holocene history of these beaches relative to the Holocene sea-level evolution. Additionally, we visited the strandplain within Pozm bay, between Pozm and Gurdim villages (Fig. 1), where we sampled and dated beach ridges at several intervals in order to understand the amount of beach progradation in the bay. We also measured a topographic profile through the beach ridge succession with a hand-held GPS (vertical error: 20% of the measure (source: Garmin)) (supplementary table S1.2-3). Additional field pictures can be found in the data repository [54].

3.2 Dating

At Pozm bay, we sampled shells from within the abandoned beach ridges. We also sampled a beach ridge deposit situated as close as possible to the Holocene paleocliff for OSL dating. At Beris beach, we sampled the oldest (most northern) part of the beach for both radiocarbon and OSL, in order to get an idea on the timing of the start of beach deposition. The OSL sample was taken directly at the foot of the Holocene paleocliff, carved within Tertiary marls.

Within the sedimentary logs, we sampled for both radiocarbon and OSL where we observed significant changes in facies in order to put timings on the events responsible for the changes. RN16-29 was sampled in life position, however other samples could not be sampled in life position, due to the nature of the facies in which they were sampled. Therefore, an overestimation of the real age of the deposit due to shell sample reworking is possible.

3.2.1 Radiocarbon dating

Aragonite shell samples were collected from the deposits for radiocarbon dating. We studied the samples in the lab with SEM secondary electron images and analyzed them with X-ray diffraction (XRD) in order to estimate their state of recrystallization. From the XRD spectra of the sample, we were able to determine if the aragonitic shell had been partially recrystallized to calcite. We added graphite as complementary material into the sample holder when not enough shell material was available (graphite peaks do not interfere with those of calcite or aragonite). A few samples (tagged RN15-…) were sent to Beta Analytics Inc. where they were prepared, bleached and analyzed with the traditional AMS counting method. The other samples (tagged RN16-...) were sent to the laboratory of ion beam physics, at the Eidgenössische Technische Hochschule Zürich (ETHZ), where they were treated and analyzed following the methods described by Hajdas [55]. Conventional ages were calibrated with Oxcal 4.2 [56] with the calibration curves IntCal 13 and Marine 13 [57], and a delta_R value of 236±31 years, as calculated using the website http://calib.org/marine/ based on local values [58,59]. Results are presented in Table 1. Additional measurements information, XRD results and SEM images of shells can be found in [54].

3.2.2 OSL dating

For OSL dating, we targeted sandy facies, poor in shell fragments and pebbles. Foreshore and shoreface facies are described as good dating target for OSL, because complete bleaching prior to burial is likely [60,61]. Samples were taken by hammering a stainless steel tube into the sediment (tube dimensions: 4 cm diameter, 20cm length). In the lab, we removed the material that had been in contact with the light (~4 cm), and analyzed the unexposed internal part of the tube. We treated the samples with the usual preparation methods to isolate 90-150 µm quartz grains through sequential treatment with HCl, H_2O_2, sodium polytangstate density separation, Frantz magnetic separation and HF treatment.

The burial dose or equivalent dose (D_e) was determined by measuring the luminescence signals on 24 aliquots per sample (each aliquot contains ~100 grain) using the SAR protocol of Murray and

Wintle [62]. We used the Risø TL/OSL-DA-20 reader at the Institute of Earth Surface Dynamics (University of Lausanne). Results were processed with the Analyst 4.31.7 software [63]. Each aliquot was evaluated according to the following acceptance criteria: recycling ratios at 10%, maximum test dose error at 10%, maximum recuperation at 10% of the natural signal and maximum paleodose error at 20%. Only 1 out of the 120 analyzed aliquots ended up being rejected. D_e values were assessed with the central age model [64]. The radioactive elements (U, Th, K and Rb), measured using ICPMS (from ActLabs, Canada), were used in order to calculate the environmental dose with the DRAC software [65]. The reliability of the protocol and zeroing of clock at the time of deposition was assessed with a dose-recovery test [66] on 4 representative samples. We exposed the samples to natural light for 48 continuous hours before measuring the natural signals (to check the residual dose). Additionally, after artificially bleaching the sample, we measured the recovery of an artificially given dose of 300 s (~36 Gy) using the same SAR protocol. Dose recovery ratios (recovered dose/ given dose) are 0.8 to 1.01. Results are presented in Table 2. More details on measurements and age calculations are presented in [54].

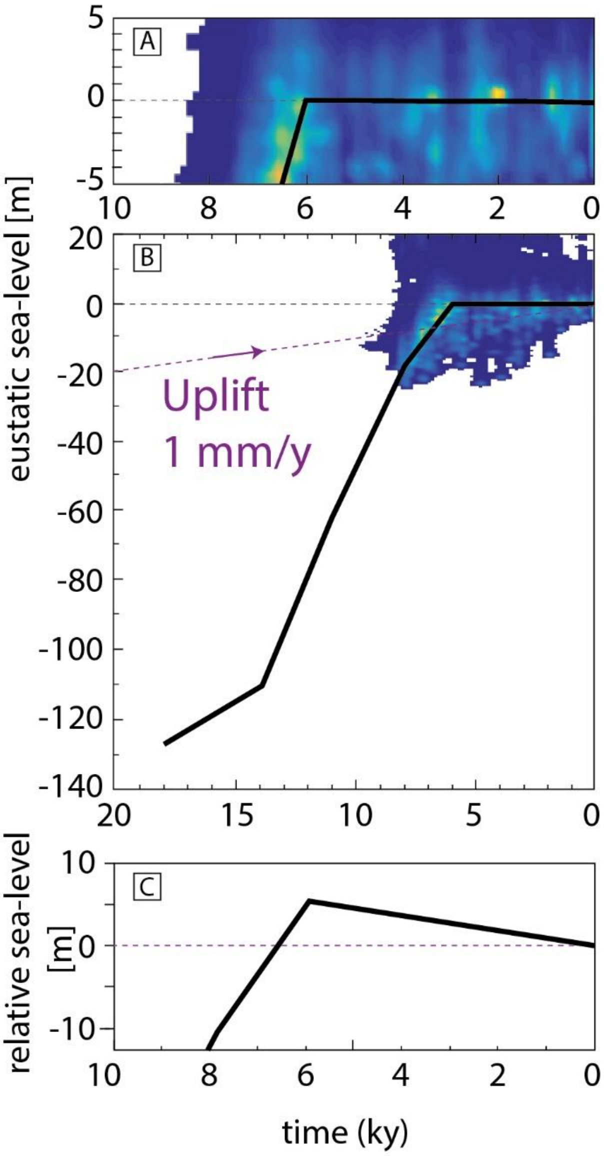

Figure 2. Simplified sea-level curve for the Holocene. (**a**) Sea-level curve of Lambeck [67] drawn with results of the monte-carlo simulation described in section 3.3. (**b**) Sea-level-time curve at different scale than shown in A. The purple line represents an uplift of 1 mm/yr. (**c**) Holocene relative sea-level changes on an uplifting coast (here, hypothetical scenario of 1 mm/yr).

3.3 Sea-level curve

Knowledge of the sea-level behavior during the Holocene is of utmost importance to study the beaches developing during this period. A number of complex sea-level curves have been published from localities around the Makran [67,68], but they are all different in their details. For our study we have focused on the simple Oman Sea curve proposed by Lambeck [68]. This curve predicts a sea-level rise until 6000 BP, where the sea level stabilized to its current position until today. Additionally, we used the sea-level marker database compiled by Hibbert et al. [69] to build a sea-level probability density plot against which we compared the curve of Lambeck [68]. We screened the database to isolate data from localities close to the Makran (Mauritius, Reunion Island, India, Sri Lanka and the Maldives) and to remove the data without a provided PRSL and error. We built the density plot using a monte carlo simulation with 10000 iterations. The age and depth values for each iteration were generated randomly following a normal distribution (for ages and Zcp) and a coral-species-specific depth distribution provided by the authors. For data not originating from coral species, we used the PRSL values provided by the database with a normal distribution. The result of the density plot closely resembles the curve of Lambeck [68], so we used this curve as an approximation of the sea-level history during the Holocene (Fig. 2). Continental uplift has an impact on the relative sea-level curve and should be taken into consideration. Figure 2c shows the relative sea-level behavior on a coast uplifting at an arbitrary value of 1 mm/yr.

3.4 Calculation of Holocene uplift rates

To calculate mean uplift rates for small time scales such as the Holocene, we have to know the altitude relative to mean sea-level at which the sampled material deposited in order to get a precise estimation of vertical displacement. For this, we use the method presented in Rovere et al. [70] combined to the general uplift formula of Lajoie [71];

$$U = (E\text{-}RWL\text{-}e)/A \tag{1}$$

where U is the mean uplift rate, E is the current elevation of the sample, RWL is the mean altitude relative to mean sea-level at which the sample deposited, e is the eustatic correction (see Fig. 2) and A is the age.

Based on the method of Rovere et al. [70], we estimated the upper limit (U_l), lower limit (L_l), indicative range (IR) and reference water level (RWL) of beach and lagoonal deposits of the Makran, which we use for uplift rate calculations. For beach deposits, a good sea-level marker is the interface between intertidal sediments and the eolian sand cap [72,73]. However, because it could not be identified in the field near the sampled material, we use the estimates proposed by Rovere et al. [70]. Details are provided in supplementary table S1.4.

We have adapted the uplift formula to account for the errors on the different terms in order to get minimum and maximum values of uplift, or uplift ranges [74,19].

$$U_{min} = [(E - \Delta E) - U_l - e] / (A + \Delta A) \tag{2}$$

$$U_{max} = [(E + \Delta E) - L_l - e] / (A - \Delta A) \tag{3}$$

We know the errors on all terms, except that for the eustatic curve, although we recognize that the eustatic curve can be a significant source of uncertainty.

4. Results

Radiocarbon and OSL dating results are compiled in Table 1 and Table 2, respectively, and presented in Fig. 3.

Table 1. Result of radiometric dating. Details in the data repository [54].

Sample	Coordinates	Area	Shell type	Radiocarbon age Conventional ± 1σ	Radiocarbon age Calibrated ± 2σ *	Comments	Beach progradation rate
	[dd.dd°]			BP	Cal BP		m/yr
RN15-P3	25.384522°N, 60.233041°E	Pozm bay	Bivalve	590 ± 30	54 ± 54	290m f.c.**	> 0.6
RN15-P7	25.387667°N, 60.232500°E	Pozm bay	Bivalve	490 ± 30	39 ± 39	660m f.c.**	> 3.3
RN15-P15	25.394817°N, 60.230150°E	Pozm bay	Bivalve	810 ± 30	184 ± 116	1450m f.c.**	> 4.8
RN15-P18	25.397750°N, 60.228133°E	Pozm bay	Bivalve	1620 ± 30	931 ± 112	1840m f.c.**	> 0.6
RN15-24	25.429833°N, 60.434300°E	Chabahar Bay	Bivalve	4240 ± 30	4010 ± 135	1500m f.c.**	0.4
RN16-18	25.428866°N, 60.434752°E	Chabahar Bay	Bivalve	6883 ± 22	7167 ± 101		
RN16-19	25.428866°N, 60.434752°E	Chabahar Bay	Gastropod	3465 ± 20	3041 ± 121		
RN16-29	25.458804°N, 60.431895°E	Chabahar Bay	Bivalve	5969 ± 21	6138 ± 117	In life position	
RN16-34	25.439082°N, 60.431512°E	Chabahar Bay	Bivalve	5903 ± 21	6067 ± 113		
RN16-36	25.439082°N, 60.431512°E	Chabahar Bay	Bivalve	6915 ± 22	7218 ± 84		
RN16-37	25.438028°N, 60.431665°E	Chabahar Bay	Bivalve	5602 ± 21	5743 ± 115		
RN15-89	25.196317°N, 61.086100°E	Beris beach	Bivalve	4590 ± 30	4506 ± 131	460m f.c.**	0.1
RN16-11	25.219917°N, 60.984411°E	Beris beach	Gastropod	5744 ± 21	5874 ± 107		
RN16-41	25.220263°N, 60.984910°E	Beris beach	Gastropod	8200 ± 23	8432 ± 88		
RN16-44	25.220263°N, 60.984910°E	Beris beach	Bivalve	8612 ± 23	8940 ± 146		

*Calibrated using Oxcal 4.2 [56], with the curves IntCal 13 and Marine 13 [57]. Reservoir correction, Delta_R = 236±31 years for Makran, according to the website, http://calib.org/marine/

**f.c.: From the coastline

Table 2. Results of OSL dating. Details in the data repository [54].

Area	**Comments**	**Sample**	**Sample depth** [m]	**Paleodose CAM ± 1σ** [Gy]	**N° of Aliquots** out of 24	**RSD** %	**OD** %	**U** ppm	**Th** ppm	**K** %	**Rb** ppm	**Water content** %	**Env. dose** [Gy / ka]	**Age ± 1σ** [a]
Pozm Bay	7km from the coastline	RN17-28	0.5 ± 0.1	2.710 ± 0.121	23	22.3	20	1.2 ± 0.05	3 ± 0.11	0.714 ± 0.02	24 ± 1.8	2 ± 2	1.386 ± 0.04	1955 ± 101
Chabahar bay	K3, Above FS	RN17-35	0.5 ± 0.1	4.489 ± 0.206	24	23.6	21	1.4 ± 0.06	3.7 ± 0.14	0.672 ± 0.02	24 ± 1.8	2 ± 2	1.438 ± 0.04	3123 ± 163
Chabahar bay	K6, Below FS	RN17-36	0.7 ± 0.2	4.368 ± 0.230	24	21.0	25	1.2 ± 0.05	3.7 ± 0.14	0.664 ± 0.02	25 ± 1.9	2 ± 2	1.371 ± 0.03	3187 ± 186
Chabahar bay	K11	RN17-37	2 ± 0.5	2.287 ± 0.073	24	17.2	15	2.3 ± 0.1	2.9 ± 0.11	0.498 ± 0.01	16 ± 1.2	2 ± 2	1.369 ± 0.03	1670 ± 67
Beris beach	At the base of the cliff	RN17-44	0.3 ± 0.1	5.929 ± 0.242	24	23.1	19	3.1 ± 0.13	2 ± 0.07	0.241 ± 0.01	11 ± 0.8	2 ± 2	1.296 ± 0.04	4576 ± 227

4.1 Fluvial sedimentary input

One of the major factors controlling the development and progradation of the coast is the sedimentary budget. We infer that the sedimentary input in the Makran mainly originates from 4 sources e.g., [75,45,76,77,73,78]; (1) alongshore transport of sea-floor sediments, (2) erosion of nearby headlands, (3) eolian transport and (4) river input. These sources are all linked to climatic conditions, which remained relatively constant in the Makran since the start of the Holocene. However, we observed the presence of ancient river channels within the low coastal plain (Fig. 4a, 4b) indicating that the Makran Rivers might have switched from one bay to another throughout the Holocene, drastically modifying the sedimentary budget locally. We gathered information on river watersheds in order to understand where fluvial sediments input the Oman Sea and how fluvial sedimentary input can influence beach progradation. We used a ASTER DEM (30m), which we analyzed using the Topotoolbox from matlab [79,80]. A presentation of river input into the Oman Sea near the Chabahar region is presented in Fig. 4a.

The eastern bay of Jiwani receives a major part of the Makran fluvial input since it hosts the mouths of both the Dasht and Pishin watersheds, with drainage areas respectively of 29000 km^2 and 20600 km^2 (second and third largest of the Makran). Beris beach receives fluvial input from small watersheds, each less than 80 km^2. Chabahar bay is currently only fed by two small watersheds, of max. 500 km^2. Pozm bay, however, is receiving sediments from two major rivers, the Nikshar and Sergan rivers, with watersheds of 5400 and 1115 km^2, respectively. Ancient river channels suggest that the Nikshar and Sergan rivers might have flown towards Gurdim and Chabahar bays, respectively, at some point during the Holocene. The majority of the sand-sized material brought into the Oman Sea by the rivers comes from erosion of the Makran ranges, northwards of the coastal plain (Fig. 4a brown numbers). In this respect, small watersheds, mostly draining the fine-grained bedrock of the coastal plain, bring little coarse material to build beaches.

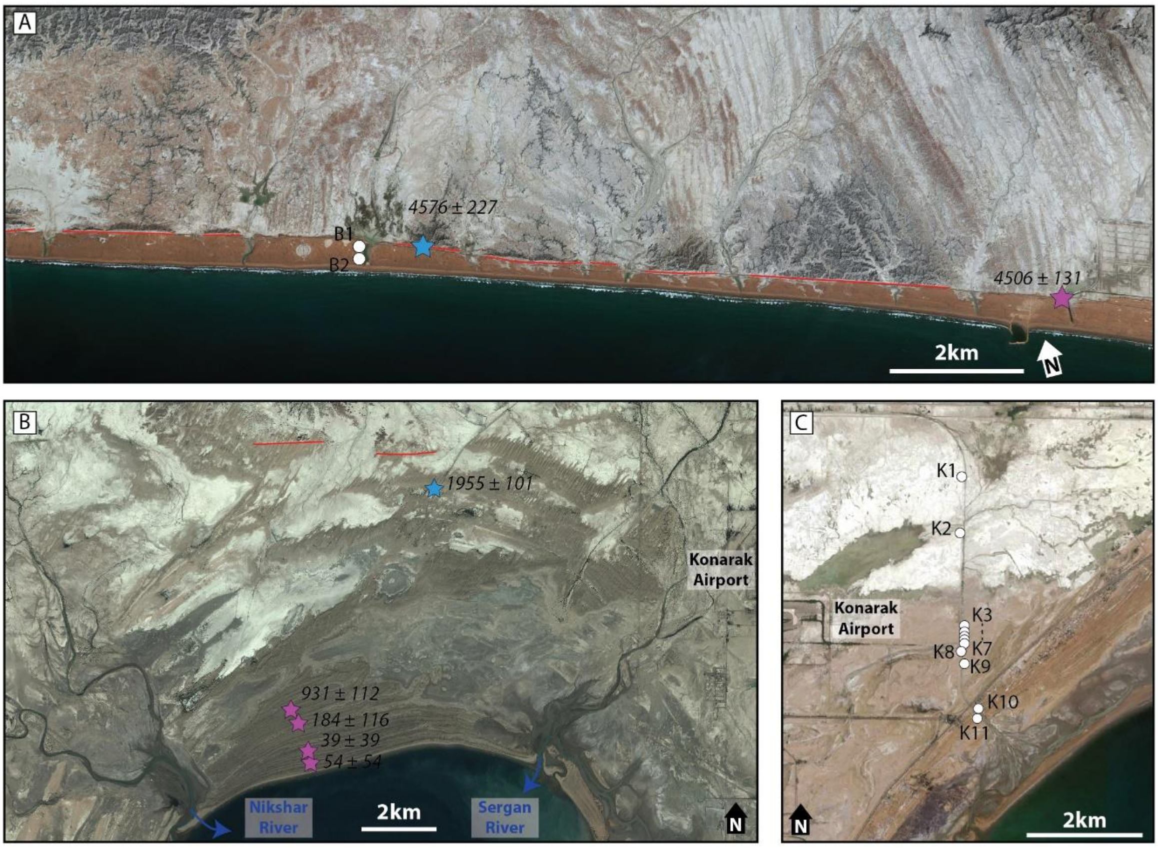

Figure 3. Satellite images of the studied beaches and localization of sampled material and measured logs. Legend: Blue star : OSL sample. Purple star: radiocarbon sample, white circles: stratigraphic logs positions, red lines: paleocliff of the mid-Holocene maximum transgression. (**a**) Beris beach, localization of the stratigraphic logs B1 and B2 and the dated samples (this study). Image from Google Earth (**b**) Pozm bay, localization of the dated samples. Image from Bing satellite. (**c**) Chabahar bay, localization of the stratigraphic logs K1-K11, along a man-made trench near Konarak airport. Image from Google Earth.

4.2 Beach geomorphology

Along the Makran coast, the important contrast in rock resistance between the two main outcropping lithologies (sandstones and marls) has promoted the development of headlands and bay-beaches, e.g., [77,81,78]. Wave action erodes faster through soft marl bedrock than through indurated sandstones, which causes the coastline to develop into deep bays and protruding headlands. Material eroded from headlands, exposed to wave attack, is transported by alongshore currents and preferentially redeposited in embayments, together with continental fluvial input, to form prograding beaches [78,77].

The presence of headland and bays favors the formation of a concave beach morphology in the shadow zones behind headlands (Fig. 1). These crenulated beaches best develop when waves approach the coastline with a steep angle of incidence and are facing towards the main alongshore current direction [82,83]. Most bay-beaches of the western Makran are crenulated, facing towards the west, implying a dominant wave direction towards the NW throughout the Late Holocene, as recently measured in Chabahar by [50] (Fig. 1, west of Pasabander). Consequently, from this dominant wave direction, alongshore currents are expected to flow from east to west [75]. Interestingly, the crenulated bays of the eastern Makran (Pakistan; Fig. 1 east of Jiwani) face in the opposite direction, suggesting a mirrored wave and alongshore regime.

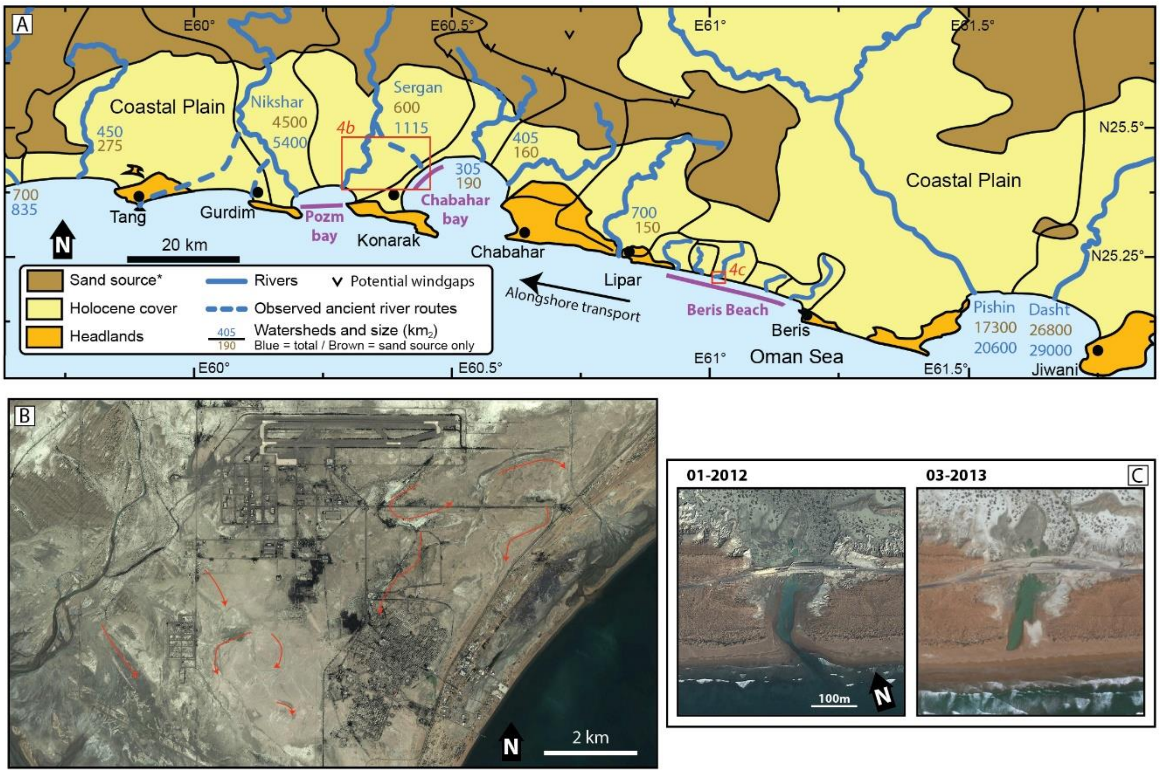

Figure 4. Fluvial input in the Chabahar region. (**a**) Map of Chabahar region with the watersheds contours. Total watershed size is expressed in blue, whereas the watershed area of hard tertiary bedrock (sand source for beaches) is expressed in brown. Purple = studied regions. *Outcropping rocks estimated to be the source of sand-sized material delivered in the Oman Sea by rivers. (**b**) Google Earth satellite image near Konarak airport. Ancient river paths are visible in the landscape (some outlined with red arrows), implying that the Sergan river used to flow into Chabahar bay. (**c**) The succession of satellite images shows that the evolution of the beach at the river mouth is influenced by floods. The river bursts through the beach ridge during floods and is re-built by the waves between flood events. N25.209° E61.022°. Images from Google Earth.

4.2.1 Beris beach

Beris beach is 30km long and is built on Tertiary marl bedrock between two rocky headlands (Fig. 1, Fig. 3a). Since re-occupation of the coastline by the sea in the Early Holocene, rapid wave erosion of the bedrock marls has taken place, forming a bay bordered by more resistant headlands [77,78]. The high marl cliffs that punctuate the back of this beach stand as relicts of the maximum extend of coastal regression that peaked shortly before ~4500 BP, according to our dating results (see below). Since then, relative sea-level fall has favored beach progradation. Its characteristic seaward-concave plan shape (eastern end) is the result of beach building by wave refraction around Beris headland under a NW predominant wave direction [83,82].

At Beris beach, the oldest beach ridge was sampled at two different locations and dated with two different methods that both yielded an age of ~4500 BP indicating the start of beach build up at that time. The OSL sample (RN17-44) was sampled at the base of the paleocliff, such that it should correctly estimate the start of beach deposition. Previous dating results from this beach include ages at 3976 ± 29 and 3646 ± 17 BP [48] and 7605 ± 75 BP [10]. The latter, significantly older than other results, is from dating of a lithofaga mollusk found within a boulder that might have been reworked during the transgression. The top sample of B1, dated at 5744 ± 21 BP also postdates the supposed age of the first beach ridge but still indicates, together with the other results cited, that Beris beach was deposited and has prograded after the mid-Holocene highstand.

The beach receives minor fluvial sedimentary input (Fig. 4a) and as a result, has remained narrow (250-600m wide, Fig. 3a) and has prograded slowly (< 0.1 m/yr) since the mid-Holocene highstand. Other sedimentary sources could be alongshore transport (two large watersheds flow into the nearby Jiwani bay) and erosion of the bordering Beris and Lipar headlands, but the distinctive dark orange color of this beach indicates that most of the sand seems to originate from the orange-colored rocks that outcrop northwards of the beach (Fig. 3a). The western part of the beach is nearly linear and is intermittently cross cut by river channels hosting lagoons (Fig. 3a, Fig. 4c). Looking over a succession of satellite images covering several years, we can see that the river incises through the beach during flash floods, whereas wave action re-builds a continuous beach ridge shortly after the flood events (Fig. 4c).

4.2.2 Chabahar bay

Chabahar bay is a 20km wide and 17 km deep omega-shaped bay situated between the two prominent headlands of Chabahar and Konarak (Fig. 1). The onshore central part of the bay is occupied by an up to 5 km wide plain of prograding beach ridges flanked by two lagoonal systems on its eastern and western sides. Similar to Beris beach, the bay-headland configuration appears to be due to contrasting rock strengths between the bay (marl) and headland (sandstone). The omega shape of the bay is due to wave diffraction around the two headlands, similar to what can be observed, in a smaller scale, behind human made breakwaters originally separated from the coastline [84]. Hence, it is possible that the rocky headlands of Konarak and Gurdim were detached from the main land at the start of the Holocene as has been proposed by others [2,18,49,29].

Although the presence of this wide strandplain hints towards a high input of sediment, Chabahar bay currently receives sediments from only two small watersheds draining mainly the fined-grained rocks of the coastal plain (Fig. 4a). Part of the sand sedimentary input comes from the erosion of the nearby headlands (mainly Chabahar headland, due to its size, upstream position and sandstone dominated bedrock). The ancient river channels observable around Konarak airport (Fig. 4b) suggest that the Sergan River used to flow into the Chabahar bay, nearly tripling the fluvial coarse-grained input. Results from Gharibreza [29] indicate that beach progradation in Chabahar bay substantially slowed down at 1200 BP, which might be the moment when the Sergan river diverted towards Pozm bay. However, recent results of Shah-Hosseini et al. [28] suggest an opposite scenario, where beach progradation increases until today. We also observed potential wind gaps in the Makran Ranges north of Chabahar, hinting towards ancient river routes towards the Chabahar bay (Fig. 4a). However, these routes were probably diverted due to rock uplift, on timescales greater than the Holocene.

4.2.3 Pozm Bay

Pozm bay is another omega-shaped bay delimited in the east by Konarak and in the west by Gurdim headlands. The size of the bay (12 km wide, 6.5 km deep) is considerably smaller than that of the neighboring Chabahar bay. However, the paleocliff, that we observed within the Tertiary marl bedrock, is 9.4 km away from the current coastline (red line, Fig. 3c), implying an important coastal progradation. The oldest ridges, situated further from the sea, are partially degraded to elongated and NNE directed eolian dunes, as expected from the two main wind directions, coming from the west and south [50]. The lowlands between the oldest ridges, possibly ancient intertidal lagoons, are transformed into ponds shortly after flash flood events, where fine-grained alluvial deposits decant. Finally, the outer 4 km of the bay hosts a succession of beach ridges, flanked by two active lagoonal systems at the mouths of the Nikshar and Sergan rivers (Fig. 3b, Fig. 4a).

We have dated four shell samples from the beach ridges at Pozm bay (from the sea, beach ridge N°3, 7, 15 and 18) (Fig. 3b) to better understand the prograding history of the strandplain. Unfortunately, the two first samples yielded very young conventional ages that could not be accurately calibrated. Nonetheless, we know they should be recent, (a maximum of several hundred years). The 15th and 18th beach ridges yielded calibrated ages of 184 ± 116 BP and 931 ± 112 BP respectively. We also sampled one of the oldest beach ridges, close to the observed paleocliff, which yielded an unexpectedly young OSL age of 1955 ± 101 years. We aimed to sample beach facies, but we do not exclude the possibility that we might have sampled an eolian deposit ([54], image A_1), which would yield a younger OSL age (minimum age).

Our dating results from the beach ridge succession at Pozm bay indicate three main facts. 1) According to the OSL results (RN17-28), the active beach ridge was still close to the paleocliff 1955 years ago (i.e. late after the mid-Holocene highstand) (Fig. 3b, blue star). 2) The recent progradation has been very fast, with a mean value of 5.2 m/yr between 1955 ± 101 years and 918 ± 112 years, and a minimum of 4.8 m/yr during the last 300 years. 3) Progradation rates seem to have slowed significantly between 931 ± 112 and 184 ± 116 years ago (Beach ridges P18 and P15) (400 meters in 747 years, or 0.55 m/yr). Nevertheless, a mean progradation rate of 5.2 m/yr over a long period of 1955 years is very high and indicates that this OSL age must be considered with caution (see above). The rapid recent (<300 years) beach progradation is probably due to a local increase in fluvial sedimentary input due to the redirection of one (or both) rivers towards Pozm bay (Fig. 4a, 4b).

4.3 Beach sedimentology

The facies description and interpretation of the depositional setting is reported in supplementary table S1.5. Sedimentary logs, legends and field pictures are compiled in Fig. 5 and Fig. 7. Additional field pictures can be found in [54], as referred to in supplementary table S1.5. Sedimentary facies at Beris beach are greatly influenced by fluvial input, as coarse conglomerate deposits constitute a substantial proportion of the sedimentary succession. In Chabahar bay, the sedimentation is dominated by lagoonal, tidal and beach deposits. Because the Makran climate has remained roughly the same for at least the last 5000 years [45,44,46], we base our facies interpretations on observation of the modern system (Fig. 6, Fig. 8) ([54], images D).

The samples from within the sedimentary successions (B1,B2 and K1 to K11) yielded complex dating results. OSL and radiocarbon results do not always agree with each other and reworking of some sampled material seems to have taken place. At the northernmost section within Chabahar bay (K1), a shell sampled in life position within the lower facies, situated directly above the bedrock can be considered as reliable. It was dated at 6138 ± 117 BP, which corresponds to the timing of the maximum transgression of the mid-Holocene highstand (Fig. 2).

Table 3. Short description and interpretation of the facies of Beris and Chabahar bay cross sections. More details may be found in supplementary table S1.5.

Facies	Short description	Depositional Environment
Beris		
1	Matrix supported, fine-grained laminated deposit	Lagoon
2	Conglomerate, clay matrix	Lagoon with fluvial input
3	Conglomerate, no matrix	Fluvial channel
4	Conglomerate, sandy matrix	Mouth bar
5	Well-sorted sandstone. Cross stratifications	Shoreface

6	Horizontally laminated well sorted sandstone	Beach
Chabahar bay		
A	Laminated fine-grained deposit, evaporites	Supratidal flats
B	Heavily bioturbated fine-grained deposit	Intertidal ponds
C	Sandy deposits, wavy beddings	Intertidal lagoon
D	Erosive base, channelised, bi-directional cross bedding	Tidal channel
E	Same as D, with occasional <20 cm thick mud drapes	Tidal channel
F	Same as D without the channelised morphology	Intertidal / subtidal
G	Horizontally laminated well sorted sandstone	Beach

4.3.1 Beris beach

B1 and B2 represent, respectively, the proximal and distal parts of the system, which can be inferred by their geographical position as well as by looking at their pebble content. The lower part of the sequence indicates the presence of a lagoon at 8432 ± 88 BP occasionally disturbed by flash flood events. After an erosive surface, the sedimentary succession switches to a facies with a major marine influence (richer in sand). Relative sea-level rise at that time (Fig. 2c) explains the presence of this flooding surface (FS). However, we suspect the sample from the sandy layer, dated at 8940 ± 146 BP (i.e., older than the underlying sample, see Fig. 5d) to be reworked. Following this event, the system progrades to a more proximal setting as relative sea-level starts to fall following the mid-Holocene highstand and the space created by relative sea-level rise gets filled with sediments. These sediments consist of thick conglomerates with few sand (facies 3), indicating a position within the main channel where erosion of the wave-built sandy layers occurs during successive floods (Fig. 4c, Fig. 6). The amount of pebbles decreases upwards and the proportion of sandy matrix increases as the channel migrates away through time. In the distal part of the system (B2), the environment remains marine (dominated by shoreface facies) though occasional thin conglomerate layers suggest sporadic fluvial input associated to the more proximal facies seen in B1. Finally, the upper beach facies in B1 marks the emergence of the succession after the mid-Holocene highstand, though once again, the system continued to be influenced by occasional floods. Since then, the beach has prograded to its current position as the coast uplifted and the relative sea-level fell (Fig. 2c), permitting the incision of the outcrop.

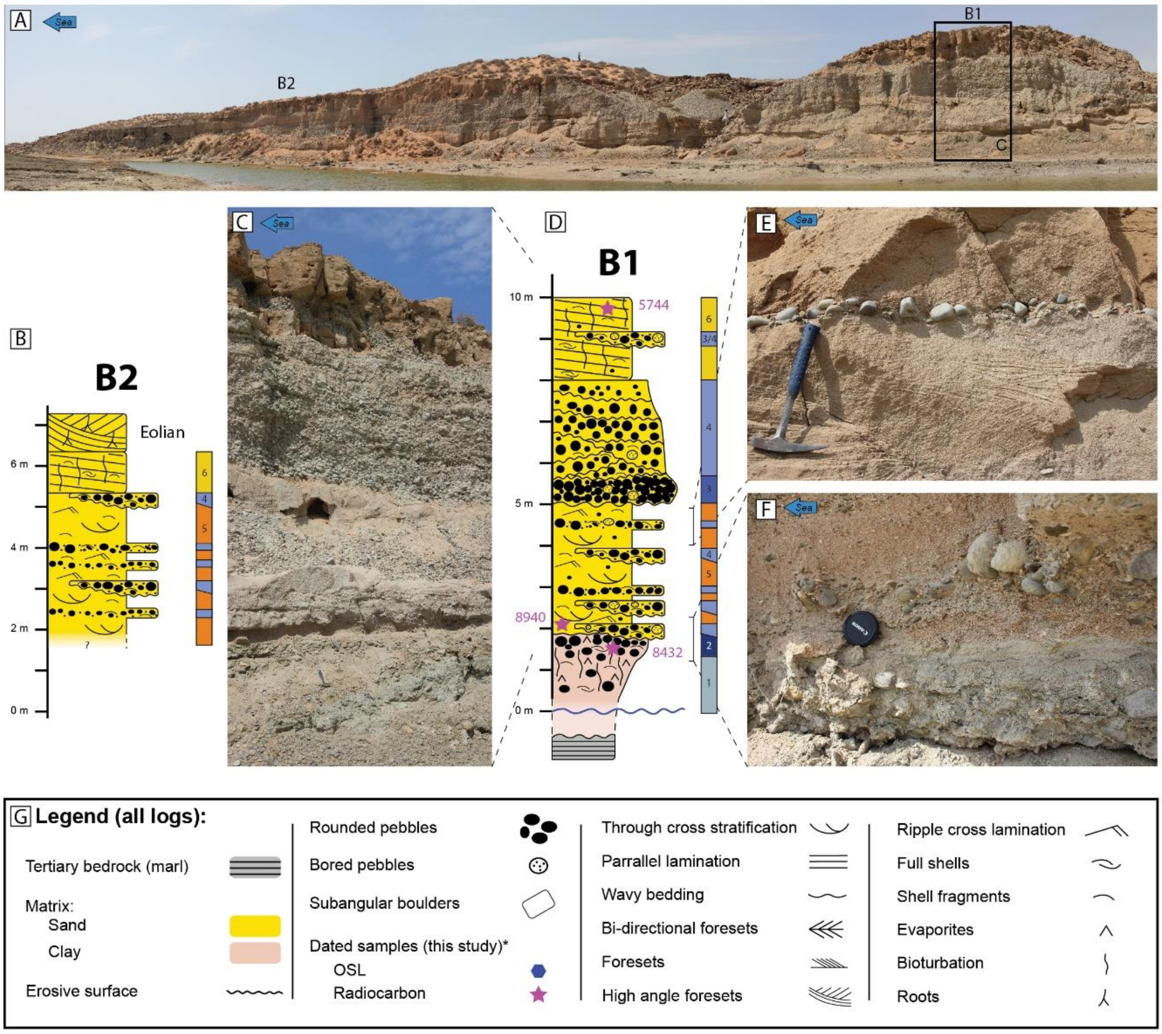

Figure 5. Beris beach stratigraphic logs. (**a**) Beris beach transect. N 25.219, E 60.985. (**b**) Log B2. (**c**) close up of the transect at the position of log B1 (black square in Fig. 5a). (**d**) Log B1. (**e**) Close up of facies 5. (**f**) Close up of the bottom of log B1, the transition from facies 2 to 4-5. (**g**) Legend for all logs (Figures 5 and 7). *Ages standard deviations are not reported on the figures but can be seen in Tables 1 and 2. More pictures can be seen in the data repository [54], images C.

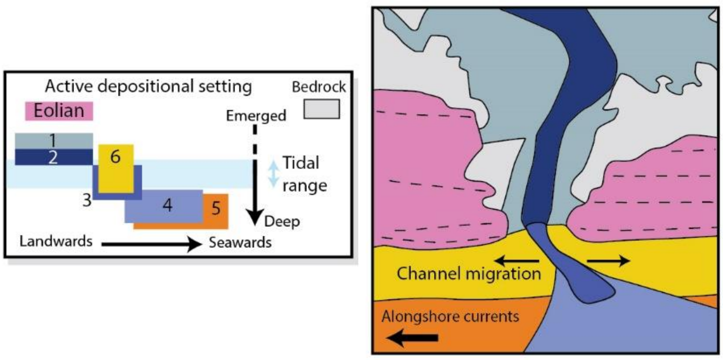

Figure 6. Beris beach, interpretation of the described facies depositional environment (based on Figure 4c). Black dashed lines: beach ridges.

4.3.2 Chabahar bay

In the proximal position of the section, the contact between the marl Tertiary bedrock and the first layers of Holocene fine-grained lagoonal deposits was observed ~5 km from the current coastline (K1). This lagoonal layer is dated at 6138 ± 117 BP on a shell in life position; hence, it was deposited during the mid-Holocene highstand. The lagoonal sediments are overlain by a thick (up to 3m observed above the surface) layer of intertidal lagoonal muds, outcropping over a lateral distance exceeding 2.5 km (K2). These deposits become progressively sandier towards the sea and about 3 km from the current coastline they are dominated by sands (K4-K8), occasionally cross cut by sandy intertidal channels rich in shell fragments (K5-K8). The layers of intertidal sediments observed in the lower part of logs K3-9 were probably deposited within the same ancient lagoonal system. Those intertidal facies are overlain by layered muds of facies A, interpreted as supratidal deposits (K3-K6, K8-9). This succession is a normal prograding sequence, as could be expected on an uplifting coast (Fig. 2c); the tidal channels are abandoned as the coastline progrades or the lagoon migrates laterally and the intertidal areas become supratidal flats (Fig. 8b).

A drastic change in facies is observed in the central portion of the sedimentary logs (K3-K9) as the supratidal layered muds of facies A abruptly transitions to the lower intertidal facies D or F (outlined blue arrows in Fig. 7, see also inset Fig. 8b). This succession is visible in most logs (K3-K9) (Fig. 7). This sedimentary succession implies the creation of accommodation following the deposition of facies A. At K9, a beach facies G overlays the supratidal facies A. Facies G is expected to form at the coastline, whereas A is deposited in a more proximal position (Fig. 8b inset), implying coastal retreat between the depositions of the two layers. Therefore, a relative sea-level rise, or flooding surface (FS), seems to occur within the sedimentary successions, whereas the relative sea-level curve of the Holocene on an uplifting coast would rather be expected to be globally falling (Fig. 2c).

We attempted to date the episode of relative sea-level rise observed within the sedimentary logs K3-K9 (FS) (outlined blue arrows in Fig. 7) in order to understand if this was a slow or fast event, or if it might coincide with the mid-Holocene maximum transgression. Unfortunately, the results are unclear, especially because OSL and radiocarbon results do not agree with each other. Therefore, we propose two different interpretations based on either method, since combining both leads to ambiguous conclusions.

Based on the radiocarbon age results, the lower layer of lagoonal deposits date shortly before the mid-Holocene highstand (~7000-6000 BP). At that time, the relative sea level was rising (Fig. 2) which seems at odds with the prograding sequence of sediments below the FS (Fig. 7a). Eventually, the sequence becomes emerged, leading to coastal regression, which is expressed in the logs by the flooding surface (FS). After the maximum transgression ~6000 years ago, the relative sea level falls, and the system progrades. Hence, the FS is associated with Early Holocene sea-level rise.

Based on OSL dating, the system postdates the mid-Holocene highstand. Samples below and above the FS date at the same age within errors of ~3150 years ago. Therefore, the prograding lagoonal system has been flooded very quickly around 3150 years ago. This rapid relative sea-level rise is at odds with the seemingly steady and undisturbed nature of the sea-level curve at that time (Fig. 2).

The seawards part of the succession is less interesting. Beach deposits, showing the characteristic low angle lamination of the swash zone, can be seen on the northern flank of the channel (K10). On the southern flank, the lower part of the K11 log is made of the supratidal muds of facies A, overlain by an erosive surface and the deposition of sandy facies rich in shells interpteted as facies D. This FS can be associated to the mid-Holocene transgression based on our dating results (Fig. 7a). The presence of decimetric subangular boulders directly above the erosive surface is attributed to ravinement.

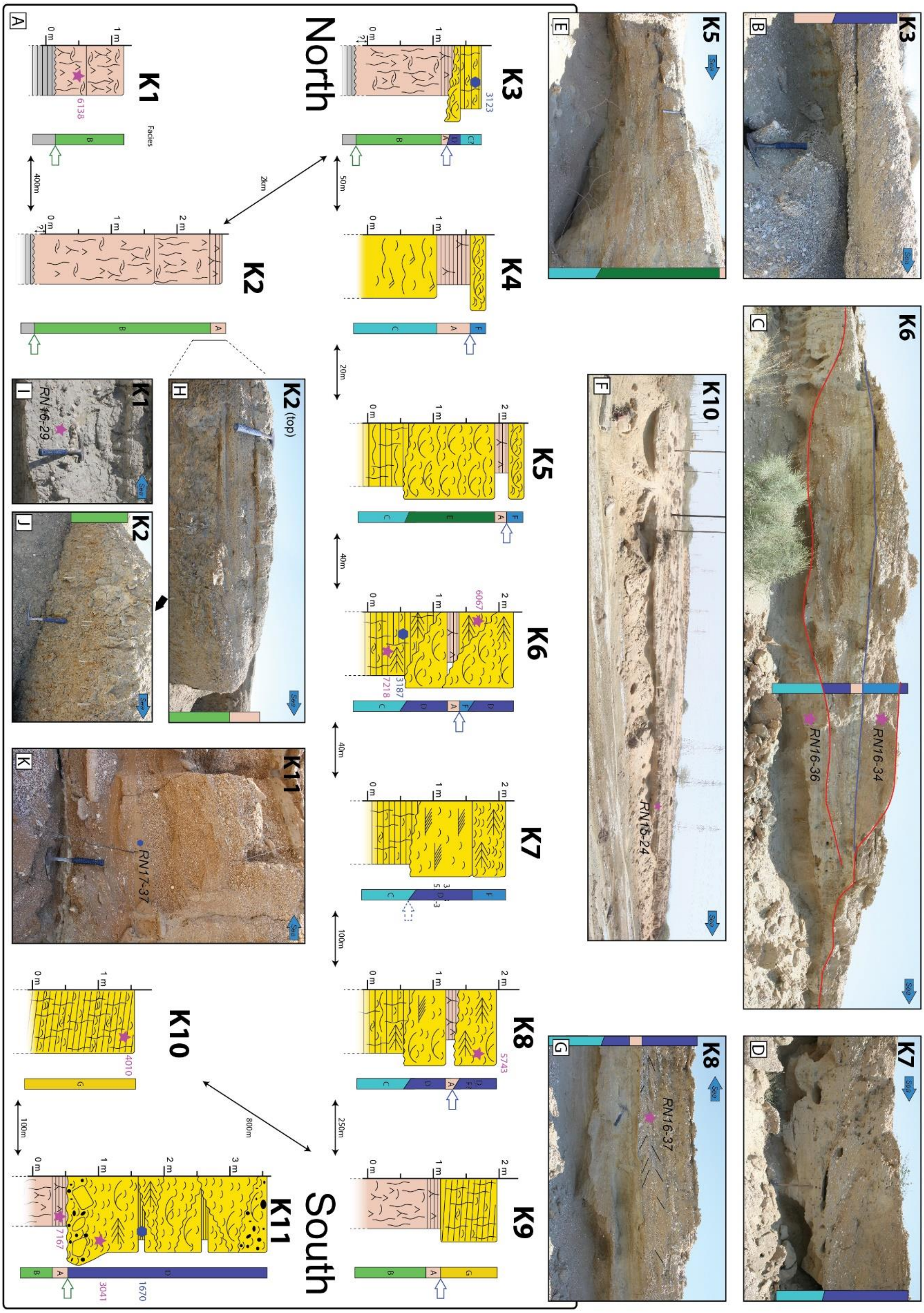

Figure 7. Stratigraphic logs of Konarak Airport section (K1-K11). Vertical scale is not absolute altitude, but height above the bottom of the channel. Blue outlined arrow: Flooding surface (see section 4.4.2). Green arrow : Mid-Holocene transgression. More field pictures can be found in the data repository [54], images B.

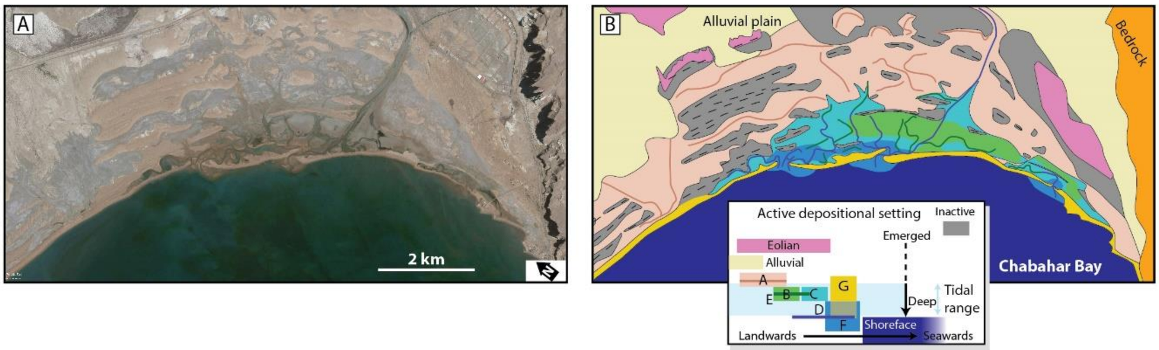

Figure 8. Chabahar bay depositional setting. (**a**) Google Earth satellite image of the eastern part of Chabahar bay (27/1/2015). N25.42°, E60.59°. (**b**) Interpretation of the described facies depositional environment. Black dashed lines: beach ridges. Colored full lines: tidal channels. Eolian degradation of inactive beach ridges is taking place but is difficult to represent graphically.

5. Discussion – Paleoseismic evidences

5.1 Signals from beach sedimentology

We believe OSL results to be more reliable because they directly date sediment deposition and are not affected by reworking issues. These results suggest that Chabahar bay may have undergone an abrupt flooding event 3150 years ago. This event might have been caused by vertical land motion caused by a great earthquake (Fig. 9e). If this was the case, the flooding surface (FS) should also be expected within the stratigraphic logs of nearby beaches. Unfortunately, the other sections studied at Beris beach do not contain sediments as young as this event. We find no clear indications for earlier vertical coseismic displacements within the Beris beach succession. The flooding surface at the base of the Beris beach sequence is contemporaneous with the Early Holocene eustatic sea-level rise and therefore does not constitute an evidence for coseismic subsidence. Moreover, most of the sedimentary facies composing the Beris section (shoreface facies, Fig. 5) do not have a close relation to the sea-level position (Fig. 6) and therefore should not be affected by minor relative sea-level changes.

From a study of altitudes of dated beach ridges, Shah-Hosseini et al. [28] constructed a relative sea-level curve of Chabahar bay. Their curve is globally falling over the Holocene, due to an overall uplifting trend of the land [19]. However, the presence of a plateau (due to a lack of data between 3200 and 2000 BP) could be caused by a subsidence event in 3150 BP, followed by uplift. Large boulders along the coast of Oman, interpreted as being displaced by tsunami waves originating in the Makran subduction zone, have been recently dated to 7540 ± 120 cal yr. BP, 1175 ± 115 cal yr. BP and 265 ± 155 cal yr. BP [85]. The 3150 year old event we describe here could complete this record.

In the eastern Makran, Page et al. [5] reported a coseismic uplift of 2m in Ormara during the 1945 Mw 8.1 earthquake, which could seem at odds with the predicted coseismic subsidence that we propose here for the western Makran. However, the general distribution of thrust coseismic vertical displacement is well known from both field observations [86–89] and numerical simulations e.g., [90,91]. The distance to the trench is an impacting factor controlling the coseismic (and interseismic) vertical deformation (Fig. 10a, green line). The trench-coast distance is smaller in the eastern than in the western Makran (~75 km in Ormara, ~130km in Chabahar) favoring coseismic uplift in the east and coseismic subsidence in the west.

5.2 Signals from beach topography

We have measured a topographic profile through Pozm bay with a hand-held GPS (Fig. 9a, 9b, 9c, supplementary table S1.2-3). The resulting topographical profile does not indicate a climbing staircase pattern as might be expected from repeated episodes of coseismic uplift. Rather, the overall flat profile probably results from normal beach progradation driven by high sediment supply e.g., [73,72]. However, three beach ridges stand out in their proportions (P2, P9 and P18), and could potentially be associated to beach sediment rework following coseismic subsidence or a tsunami e.g., [16]. P2 is one of the youngest ridges and might be associated with the tsunami of 1945. P9 is recent (< 184 ± 116 BP), but does not correspond to any known historical earthquake from the western Makran. P18 (dated at 931 ± 112 BP) could be associated with the tsunamigenic earthquake that happened in the western Makran in 1008 AD [8]. The slow in beach progradation rates that occurred between the dated samples at P18 (931 ± 112 y) and P15 (184 ± 116 y) is intriguing. It might be the effect of a sudden transgressive event before the deposition of P15, followed by resumed progradation. The topographical profile through Chabahar bay by Gharibreza [29] shows a prominent beach ridge in a seawards position of their 3481 ± 87 BP sample, which could be associated with the event 3150 years ago that produced a flooding surface within our studied sedimentary succession of Chabahar bay (section 4.3.2, Fig. 7a, Fig. 9e). Additionally, at Beris beach, we noticed a prominent beach ridge halfway between the paleocliff and the sea (yellow dashed line in Fig. 9f, see also Fig. 1). Unfortunately, this ridge was not dated.

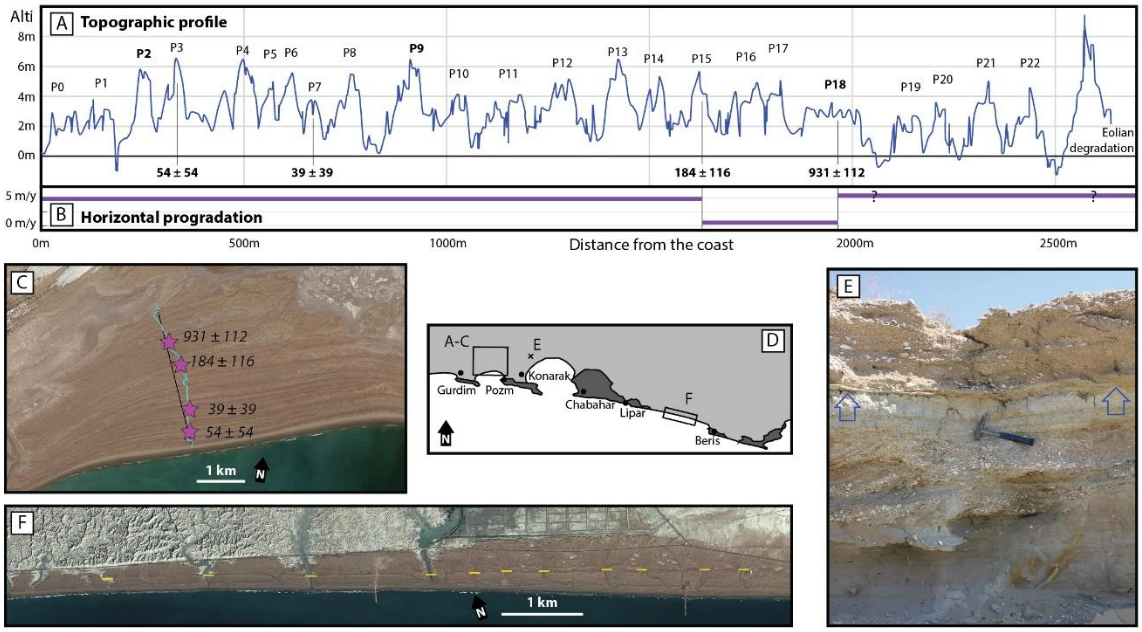

Figure 9. Paleoseismic hints in the western Makran beaches. (**a**) Topographic profile through Pozm bay-beach ridge succession (see Fig. 9c). No obvious step-like topography can be detected. (**b**) Horizontal progradation speed from dated ridges. (**c**) Satellite view of Pozm bay profile (Fig. 9a). Image Google Earth at 25.39°N, 60.24°E. The profile is projected on the black line (see supplementary table S1.3). (**d**) Geographical situation of the presented pictures. (**e**) Flooding surface (blue arrows) within the sedimentary succession of Chabahar bay that might be due to coastal subsidence, dated ~3150 years ago by OSL. 25.439082°N, 60.431817°E. (**f**) Beris beach. A prominent beach ridge, associated with a topographic step can be observed within the beach (yellow dashed line). Image Google Earth at 25.18°N, 61.10°E.

5.3 Holocene uplift rates

Rock uplift rates are of interest to try to understand the seismic behavior of the region. Short-term uplift rates, based on Holocene dates, have been observed to be very different from those obtained on longer time scales (usually from Pleistocene marine terraces) [92–94]. On a small time scale of a few thousand years, coseismic and interseismic vertical movements are a major component of the total vertical displacement [95]. Hence, in this context, the timing of sample deposition and current time position within the seismic cycle is expected to be an important factor influencing the short-term uplift rates (see Fig. 10).

Uplift calculations based on Holocene samples have been attempted by previous authors [48,29,10,5,28] and are also presented here based on our results (section 3.4, Table 3). Holocene mean uplift rates from near the middle of Beris beach are very high, varying between 2.9 and 3.75 mm/yr. These values fit quite well with the Late Pleistocene trends obtained from marine terraces [19], where long-term uplift rates along Beris beach increase from from 1 to 5 mm/yr going from west to east. Note that the uncertainties regarding the Pleistocene uplift trend along Beris beach are high due to local lack of data [19], which makes comparison to Holocene rates dubious. However, the fast Holocene uplift rates obtained here emphasize the highly active nature of tectonics in this region.

Table 4. Holocene uplift rates. Uplift rates based on lagoonal deposits are more precise due to their low IR, compared to beach deposits. More details in supplementary table S1.4.

Area	**Sample**	**Deposits**	**Age ± 2σ**	**Mean Uplift rate since Age**	**Pleistocene uplift rate [19]**
			[yr]	[mm/yr]	[mm/yr]
	RN15-24	Beach	4010 ± 135	1.29 ± 0.9	~0.6
Chabahar bay	RN16-18	Lagoon	7167 ± 101	1.88 ± 0.2	~0.6
	RN16-29	Lagoon	6138 ± 117	1.38 ± 0.4	~0.6
	RN15-89	Beach	4506 ± 131	2.92 ± 1.2	1 to 4
Beris beach	RN16-41	Lagoon	8432 ± 88	3.38 ± 0.2	1 to 4
	RN17-44 (OSL)	Beach	4576 ± 454	3.75 ± 1.8	1 to 4

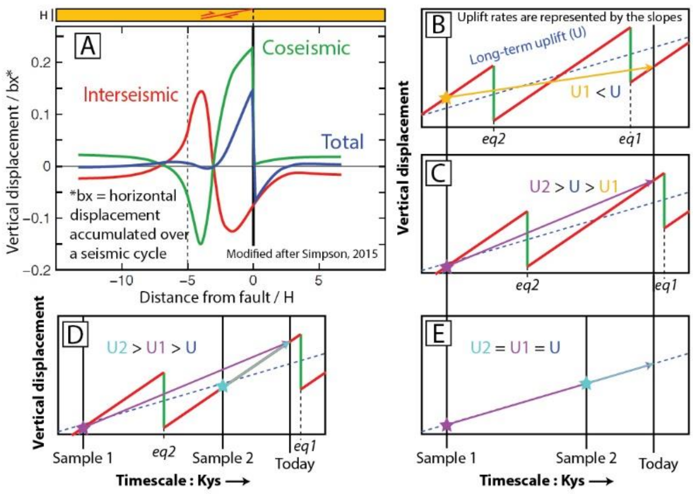

Figure 10. Scenarios of vertical displacements on a seismically active subduction zone. eq: earthquake. (**a**) Vertical deformation distribution based on a viscoelastic model of elastic rebound for a thrust earthquake [90]. Our example scenarios of Fig. 10b to 10d are at ~-5H from the trench (dashed black line), where coseismic subsidence and interseismic uplift occurs. (**b**) and (**c**) show two different scenarios, where sample deposition and current position occur at different moments within the seismic cycle. Red and green lines represent respectively the interseismic and coseismic movement of the continent (overriding plate of a subduction thrust). The short-term uplift calculated from the Holocene beach uplift (U1, U2) can potentially be very variable, as well as different from the long-term uplift calculated (from emerged marine terraces) over a multitude of seismic cycles (U). Note that today's position in the seismic cycle seems to be an important factor determining calculated short term uplift rates: If a coseismic subsidence event recently happened, we can expect U1 to be generally lower than U (Fig. 10b), and inversely (reversed behavior for coseismic uplift). Do fast Holocene rates calculated for the Makran imply an upcoming coseismic subsidence earthquake (like in Fig. 10c)? (**d**) Example showing how samples with different ages having different uplift rates

suggest a non-linear history of vertical displacements. (**e**) Example where continuous deformation happens without coseismic vertical displacements, U1, U2 and U are expected to be equal.

In Chabahar bay, previous uplift results vary substantially, ranging from 0.7 to 4.75 mm/yr [28,29]. Our mean Holocene uplift rates in the western Chabahar bay vary between 1.3 and 1.9 mm/yr. Both ours and previous results are higher than the predicted long-term trend of ~0.6 mm/yr obtained from the Konarak marine terraces situated 10 km southwards [19].

Holocene uplift rates obtained from lagoonal and beach deposits in Chabahar bay are much higher than Pleistocene uplift rates obtained from marine terraces. Moreover, within the same beach, calculated uplift rates differ, depending on the age of the considered sample (i.e., the time considered for averaging the uplift rate) (Table 4) (see Fig. 10d). This indicates a complex history of vertical movements on time scales of less than several millennia, possibly related to earthquakes. We do not currently have sufficient data to provide a clear picture of the vertical motion of this region over the Holocene. However, the fact that short-term and long-term uplift trends are different (e.g., Fig. 10b, 10c) might indicate that the Chabahar region is strongly influenced by large, infrequent earthquakes.

6. Conclusion

In this study, we have presented sedimentological data along with dating to show the evolution of the coastal Makran in Iran during the Holocene. Results from two studied beach sections indicate that since 8400 BP, the coastal region of the Makran was occupied by the sea. Coastal lagoons were progressively submerged with time until the maximum Holocene transgression. Since then, deposition was dominated by prograding sequences of tidal and beach deposits. Variation in the rate of coastal progradation during the Late Holocene seems to be strongly linked to the migration of fluvial sedimentary input from one bay to another.

Our observations are in line with what might be expected on an uplifting coast. However, some geomorphological and sedimentological singularities indicate the possible occurrence of at least one megathrust earthquake events during the Holocene. In Chabahar bay, we observed a flooding surface within the Late Holocene sedimentary succession, which we dated at 3150 years BP from two (underlying and overlying) OSL results. We attribute this sudden relative sea-level rise to coseismic subsidence. Additionally, short-term uplift rates obtained from our Holocene samples vary depending on the timescale considered, which might indicate a complex history of vertical displacements, possibly linked to earthquakes.

Supplementary Materials: The following are available online at www.mdpi.com/xxx/s1, Table S1: Published Makran beach dating results, Pozm bay GPS data, Uplift rate calculation method and observed facies descriptions. Data repository: [54], field pictures, radiocarbon dating analytical details, OSL dating analytical details.

Author Contributions: Conceptualization, Raphaël Normand and Guy Simpson; Formal analysis, Raphaël Normand, Frédéric Herman and Rabiul Haque Biswas; Funding acquisition, Guy Simpson; Investigation, Raphaël Normand, Guy Simpson, Frédéric Herman, Rabiul Haque Biswas and Abbas Bahroudi; Methodology, Raphaël Normand; Project administration, Guy Simpson and Abbas Bahroudi; Resources, Frédéric Herman and Rabiul Haque Biswas; Visualization, Raphaël Normand; Writing – original draft, Raphaël Normand; Writing – review & editing, Raphaël Normand, Guy Simpson, Frédéric Herman, Rabiul Haque Biswas and Abbas Bahroudi.

Funding: This work was funded by the Swiss National Science Foundation, project n°200021_155904.

Acknowledgments: We are grateful to Reza Ensani, Feisal Arjomandi, Nurrudin Mazarzehi, Yousef Adeeb and Gholamreza Hosseinyar for helping us with logistics in Iran and accompanying us in the field. We also would like to thank the analytical assistance of Irka Hajdas for radiocarbon dating, Agathe Martignier for SEM, Annette Süssenberger and Emanuelle Ricchi for XRD analysis.

Conflicts of Interest: The authors declare no conflict of interest.

Appendix A

If the method section is too long, we can try to arrange to put some of its content to the Appendix (e.g., sections 3.3 and 3.4).

References

1. Falcon, N. L. Raised beaches and terraces of the Iranian Makran coast. *Geogr. J.* **1947**, *109*, 149–151
2. Snead, R. J. Recent Morphological changes along the coast of West Pakistan. *Ann. Assoc. Am. Geogr.* **1967**, *57*, 550–565 doi:10.1111/j.1467-8306.1967.tb00621.x
3. Reyss, J. L., Pirazzoli, P. A., Haghipour, A., Hatté, C., & Fontugne, M. Quaternary marine terraces and tectonic uplift rates on the south coast of Iran. *Geol. Soc. London, Spec. Publ.* **1998**, *146*, 225–237 doi:10.1144/GSL.SP.1999.146.01.13
4. Byrne, D. E., Sykes, L. R., & Davis, D. M. Great Thrust Earthquakes and Aseismic Slip Along the Plate Boundary of the Makran Subduction Zone. *J. Geophys. Res. Earth* **1992**, *97*, 449–478 doi:10.1029/91JB02165
5. Page, W. D., Alt, J. N., Cluff, L. S., & Plafker, G. Evidence for the recurrence of large-magnitude earthquake along the Makran coast of Iran and Pakistan. *Tectonophysics* **1979**, *52*, 533–547 doi:10.1016/0040-1951(79)90269-5
6. Ambraseys, N. N., & Melville, C. P. *A history of Persian earthquakes*. Cambridge University Press, Cambridge, 1982, doi:10.1002/eqe.4290110412
7. Quittmeyer, R. C., & Jacob, K. H. Historical and Modern seismicity of Pakistan, Afghanistan, Northwestern India, and Southeastern Iran. *Bull. Seismol. Soc. Am.* **1979**, *69*, 773–823
8. Heidarzadeh, M., Pirooz, M. D., Zaker, N. H., Yalciner, A. C., Mokhtari, M., & Esmaeily, A. Historical tsunami in the Makran Subduction Zone off the southern coasts of Iran and Pakistan and results of numerical modeling. *Ocean Eng.* **2008**, *35*, 774–786 doi:10.1016/j.oceaneng.2008.01.017
9. Musson, R. M. W. Subduction in the Western Makran: the historian's contribution. *J. Geol. Soc. London.* **2009**, *166*, 387–391 doi:10.1144/0016-76492008-119
10. Rajendran, C. P., Rajendran, K., Shah-hosseini, M., Beni, A. N., Nautiyal, C. M., & Andrews, R. The hazard potential of the western segment of the Makran subduction zone, northern Arabian Sea. *Nat. Hazards* **2013**, *65*, 219–239 doi:10.1007/s11069-012-0355-6
11. Smith, G. L., McNeill, L. C., Wang, K., He, J., & Henstock, T. J. Thermal structure and megathrust seismogenic potential of the Makran subduction zone. *Geophys. Res. Lett.* **2013**, *40*, 1528–1533 doi:10.1002/grl.50374
12. Penney, C., Tavakoli, F., Saadat, A., Nankali, H. R., Sedighi, M., Khorrami, F., Sobouti, F., Rafi, Z., Copley, A., Jackson, J., & Priestley, K. Megathrust and accretionary wedge properties and behaviour in the Makran subduction zone. *Geophys. J. Int.* **2017**, *209*, 1800–1830 doi:10.1093/gji/ggx126
13. Darwin, C. *Geological Observations on South America*. Cambridge University Press, Cambridge, 1846, doi:10.1017/CBO9780511910180
14. Atwater, B. F., Musumi-Rokkaku, S., Satake, K., Tsuji, Y., Ueda, K., & Yamaguchi, D. K. *The Orphan Tsunami of 1700—Japanese clues to a parent earthquake in North America*. University of Washington Press, U.S. Geological Survey Professional Paper 1707, 2005, doi:10.3133/pp1707
15. McSaveney, M. J., Graham, I. J., Begg, J. G., Beu, A. G., Hull, A. G., Kim, K., & Zondervan, A. Late Holocene uplift of beach ridges at Turakirae Head, south Wellington coast, New Zealand. *New Zeal. J. Geol. Geophys.* **2006**, *49*, 337–358 doi:10.1080/00288306.2006.9515172
16. Monecke, K., Templeton, C. K., Finger, W., Houston, B., Luthi, S., Mcadoo, B. G., Meilianda, E., Storms, J. E. A., Walstra, D., Amna, R., Hood, N., Karmanocky, F. J., Rusydy, I., & Unggul, S. Beach ridge patterns in West Aceh , Indonesia , and their response to large earthquakes along the northern Sunda trench. *Quat. Sci. Rev.* **2015**, *113*, 159–170 doi:10.1016/j.quascirev.2014.10.014
17. Vita-Finzi, C. Recent coastal deformnation near the Strait of Hormuz. *Proc. R. Soc. Lond.* **1982**, *382*, 441–457 doi:10.1098/rspa.1982.0111
18. Snead, R. J. Uplifted Marine Terraces along the Makran coast of Pakistan and Iran. in *Himalaya to the Sea* ed. Shroder, J. F. J. Routledge, London, 1993, 327–362
19. Normand, R., Simpson, G., Herman, F., Biswas, R. H., Bahroudi, A., & Schneider, B. Dating and morpho-stratigraphy of uplifted marine terraces in the Makran subduction zone (Iran). *Earth Surf. Dyn.* **2019**, *7*, 321–344 doi:10.5194/esurf-7-321-2019

20. Pararas-Carayannis, G. The Potential of Tsunami Generation along the Makran Subduction. *Sci. Tsunami hazards* **2006**, *24*, 358–384
21. Hafeez, H. The potential of tsunami generation along Karachi and the Makran coast of Pakistan. *Pakistan J. Meteorol.* **2007**, *4*, 25–40 doi:10.1007/s10661-018-7048-x
22. Rajendran, C. P., Ramanamurthy, M. V., Reddy, N. T., & Rajendran, K. Hazard implications of the late arrival of the 1945 Makran tsunami. *Curr. Sci.* **2008**, *95*, 1739–1743
23. Heidarzadeh, M., & Kijko, A. A probabilistic tsunami hazard assessment for the Makran subduction zone at the northwestern Indian Ocean. *Nat. Hazards* **2011**, *56*, 577–593 doi:10.1007/s11069-010-9574-x
24. Schneider, B., Hoffmann, G., & Reicherter, K. Scenario-based tsunami risk assessment using a static flooding approach and high-resolution digital elevation data: An example from Muscat in Oman. *Glob. Planet. Change* **2016**, *139*, 183–194 doi:10.1016/j.gloplacha.2016.02.005
25. Hoffmann, G., Reicherter, K., Wiatr, T., Grützner, C., & Rausch, T. Block and boulder accumulations along the coastline between Fins and Sur (Sultanate of Oman): tsunamigenic remains? *Nat. Hazards* **2013**, *65*, 851–873 doi:10.1007/s11069-012-0399-7
26. Donato, S. V., Reinhardt, E. G., Boyce, J. I., Pilarczyk, J. E., & Jupp, B. P. Particle-size distribution of inferred tsunami deposits in Sur Lagoon, Sultanate of Oman. *Mar. Geol.* **2009**, *257*, 54–64 doi:10.1016/j.margeo.2008.10.012
27. Shah-Hosseini, M., Morhange, C., Naderi Beni, A., Marriner, N., Lahijani, H., Hamzeh, M., & Sabatier, F. Coastal boulders as evidence for high-energy waves on the Iranian coast of Makran. *Mar. Geol.* **2011**, *290*, 17–28 doi:10.1016/j.margeo.2011.10.003
28. Shah-Hosseini, M., Ghanavati, E., Morhange, C., Naderi Beni, A., Lahijani, H. A., & Hamzeh, M. A. The evolution of Chabahar beach ridge system in SE Iran in response to Holocene relative sea level changes. *Geomorphology* **2018**, *318*, 139–147 doi:10.1016/j.geomorph.2018.06.009
29. Gharibreza, M. Evolutionary trend of paleoshorelines in the Coastal Makran zone (Southeast Iran) since the mid-Holocene. *Quat. Int.* **2016**, *392*, 203–212 doi:10.1016/j.quaint.2015.06.030
30. Gharibreza, M. R., & Motamed, A. Late Quaternary Paleoshorelines and Sedimentary Sequences in Chabahar Bay (Southeast of Iran). *J. Coast. Res.* **2006**, *226*, 1499–1504 doi:10.2112/05A-0020.1
31. Zare, M., Amini, H., Yazdi, P., Sesetyan, K., Demircioglu, M. B., Kalafat, D., Erdik, M., Giardini, D., Khan, M. A., & Tsereteli, N. Recent developments of the Middle East catalog. *J. Seismol.* **2014**, *18*, 749–772 doi:10.1007/s10950-014-9444-1
32. Smith, G., McNeill, L., Henstock, I. J., & Bull, J. The structure and fault activity of the Makran accretionary prism. *J. Geophys. Res. Solid Earth* **2012**, *117*, 1–17 doi:10.1029/2012JB009312
33. Vernant, P., Nilforoushan, F., Hatzfeld, D., Abbassi, M. R., Vigny, C., Masson, F., Nankali, H., Martinod, J., Ashtiani, A., Bayer, R., Tavakoli, F., & Chéry, J. Present-day crustal deformation and plate kinematics in the Middle East constrained by GPS measurements in Iran and northern Oman. *Geophys. J. Int.* **2004**, *157*, 381–398 doi:10.1111/j.1365-246X.2004.02222.x
34. Masson, F., Anvari, M., Djamour, Y., Walpersdorf, A., Tavakoli, F., Daignières, M., Nankali, H., & Van Gorp, S. Large-scale velocity field and strain tensor in Iran inferred from GPS measurements: New insight for the present-day deformation pattern within NE Iran. *Geophys. J. Int.* **2007**, *170*, 436–440 doi:10.1111/j.1365-246X.2007.03477.x
35. Khan, M. A., Bendick, R., Bhat, M. I., Bilham, R., Kakar, D. M., Khan, S. F., Lodi, S. H., Qazi, M. S., Singh, B., Szeliga, W., & Wahab, A. Preliminary geodetic constraints on plate boundary deformation on the western edge of the Indian plate from TriGGnet (Tri-University GPS Geodesy Network). *J. Himal. Earth Sci.* **2008**, *41*, 71–87
36. Vita-Finzi, C. Neotectonics in the Arabian Sea coasts. *Geol. Soc. London, Spec. Publ.* **2002**, *195*, 87–96 doi:10.1144/GSL.SP.2002.195.01.06
37. Burg, J.-P., Dolati, A., Bernoulli, D., & Smit, J. Structural style of the Makran Tertiary accretionary complex in SE-Iran. in *Lithosphere Dynamics and Sedimentary Basins: The Arabian Plate and Analogues* eds. Al Hosani, K., Roure, F., Ellison, R. & Lokier, S. Springer, 2012, 239–259 doi:10.1007/978-3-642-30609-9_12
38. McCall, G. J. H. A summary of the geology of the Iranian Makran. *Geol. Soc. London, Spec. Publ.* **2002**, *195*, 147–204 doi:10.1144/GSL.SP.2002.195.01.10
39. Harrison, J. V. Coastal Makran : Discussion. *Geogr. J.* **1941**, *97*, 1–15
40. Harms, J. C., Cappel, H. N., & Francis, D. C. The Makran Coast of Pakistan: It's Stratigraphy and Hydrocarbon Potential. in *Marine Geology and Oceanography of Arabian Sea and Coastal Pakistanography of*

Arabian Sea and Coastal Pakistan eds. Haq, B. U. & Milliman, J. D. Van Nostrand Reinhold Company Inc., 1984, 3–26

41. Ghorashi, M. Late Cainozoic faulting in S.E. Iran. PhD Thesis, University College London, 1978,
42. Blanford, W. T. Note on the geological formations seen along the coasts of Bilúchístán and Persia from Karáchí to the head of the Persian Gulf, and on some of the Gulf Islands. *Rec. Geol. Surv. India* **1872**, *5*, 41–45
43. Stiffe, A. W. On the Mud-craters and Geological Structure of the Mekran Coast. *Q. J. Geol. Soc. London* **1874**, *30*, 50–53 doi:10.1144/GSL.JGS.1874.030.01-04.24
44. Ivory, S. J., & Lézine, A. M. Climate and environmental change at the end of the Holocene Humid Period: A pollen record off Pakistan. *Comptes Rendus - Geosci.* **2009**, *341*, 760–769 doi:10.1016/j.crte.2008.12.009
45. Prins, M. A., Postma, G., Cleveringa, J., Cramp, A., & Kenyon, N. H. Controls on terrigenous sediment supply to the Arabian Sea during the late quaternary: The Indus fan. *Mar. Geol.* **2000**, *169*, 327–349 doi:10.1016/S0025-3227(00)00086-4
46. Bourget, J., Zaragosi, S., Ellouz-Zimmermann, S., Ducassou, E., Prins, M. A., Garlan, T., Lanfumey, V., Schneider, J. L., Rouillard, P., & Giraudeau, J. Highstand vs. lowstand turbidite system growth in the Makran active margin: Imprints of high-frequency external controls on sediment delivery mechanisms to deep water systems. *Mar. Geol.* **2010**, *274*, 187–208 doi:10.1016/j.margeo.2010.04.005
47. Sanlaville, P., Besenval, R., Evin, J., & Prieur, A. Evolution de la région littorale du Makran pakistanais à l'Holocène. *Paléorient* **1991**, *17*, 3–18 doi:10.3406/paleo.1991.4536
48. Haghipour, N., Burg, J. P., Ivy-Ochs, S., Hajdas, I., Kubik, P., & Christl, M. Correlation of fluvial terraces and temporal steady-state incision on the onshore Makran accretionary wedge in southeastern Iran: Insight from channel profiles and 10Be exposure dating of strath terraces. *Bull. Geol. Soc. Am.* **2014**, *127*, 560–583 doi:10.1130/B31048.1
49. Little, R. D. Terraces of the Makran Coast of Iran and parts of West Pakistan. PhD Thesis, University of Southern California, 1972,
50. Saket, A., & Etemad-shahidi, A. Wave energy potential along the northern coasts of the Gulf of Oman , Iran. *Renew. Energy* **2012**, *40*, 90–97 doi:10.1016/j.renene.2011.09.024
51. Saket, A., Etemad-shahidi, A., & Moeini, M. H. Evaluation of ECMWF wind data for wave hindcast in Chabahar zone. *J. Coast. Res.* **2013**, 380–385 doi:10.2112/SI65-065.1
52. Vita-Finzi, C. 14C Dating of recent crustal movements in the Persian Gulf and Iranian Makran. *Radiocarbon* **1980**, *22*, 763–773 doi:10.1017/S0033822200010134
53. Sanlaville, P., & Dalongeville, R. L'évolution des espaces littoraux du golfe Persique et du golfe d'Oman depuis la phase finale de la transgression post-glaciaire. *Paléorient* **2018**, *31*, 9–26 doi:10.3406/paleo.2005.4780
54. Normand, R., Simpson, G., Herman, F., Biswas, R. H., & Bahroudi, A. Data for: Holocene coastal evolution of the eastern Iranian Makran: Insights on seismic activity based on beach morphology and sedimentology. **2019**, doi:10.5281/zenodo.2558320
55. Hajdas, I. Radiocarbon dating and its applications in Quaternary studies. *Quat. Sci. J. - Eiszeitalter und Gegenwart* **2008**, *57*, 2–24 doi:10.3285/eg.57.1-2.1
56. Bronk Ramsey, C., & Lee, S. Recent and Planned Developments of the Program OxCal. *Radiocarbon* **2013**, *55*, 720–730 doi:10.2458/azu_js_rc.55.16215
57. Reimer, P. *et al.* IntCal13 and Marine13 Radiocarbon Age Calibration Curves 0–50,000 Years cal BP. *Radiocarbon* **2013**, *55*, 1869–1887 doi:10.2458/azu_js_rc.55.16947
58. Southon, J., Kashgarian, M., Fontugne, M., Metivier, B., & Yim, W. W.-S. Marine reservoir correction for the Indian Ocean an Southeast Asia. *Radiocarbon* **2002**, *44*, 167–180 doi:10.1017/S0033822200064778
59. von Rad, U., Schaaf, M., Michels, K. H., Schulz, H., Berger, W. H., & Sirocko, F. A 5000-yr Record of Climate Change in Varved Sediments from the Oxygen Minimum Zone off Pakistan, Northeastern Arabian Sea. *Quat. Res.* **1999**, *51*, 39–53 doi:10.1006/qres.1998.2016
60. Murray, A. S., & Olley, J. M. Precision and accuracy in the optically stimulated luminescence dating of sedimentary quartz: A status review. *Geochronometria* **2002**, *21*, 1–16
61. Lamothe, M. Luminescence dating of interglacial coastal depositional systems : Recent developments and future avenues of research. *Quat. Sci. Rev.* **2016**, *146*, 1–27 doi:10.1016/j.quascirev.2016.05.005
62. Murray, A. S., & Wintle, A. G. Luminescence dating of quartz using an improved single-aliquot regenerative-dose protocol. *Radiat. Meas.* **2000**, *32*, 57–73 doi:10.1016/S1350-4487(99)00253-X

63. Duller, G. A. T. The Analyst software package for luminescence data : overview and recent improvements. *Anc. TL* **2015**, *33*, 35–42
64. Galbraith, R. F., Roberts, R. G., Laslett, G. M., Yoshida, H., & Olley, J. M. Optical dating of single and multiple grains of quartz from Jinmium rock shelter, Northern Australia: Part I, Experimetal design and statistical models. *Archaeometry* **1999**, *41*, 339–364 doi:10.1111/j.1475-4754.1999.tb00987.x
65. Durcan, J. A., King, G. E., & Duller, G. A. T. DRAC : Dose Rate and Age Calculator for trapped charge dating. *Quat. Geochronol.* **2015**, *28*, 54–61 doi:10.1016/j.quageo.2015.03.012
66. Murray, A. S., & Wintle, A. G. The single aliquot regenerative dose protocol: Potential for improvements in reliability. *Radiat. Meas.* **2003**, *37*, 377–381 doi:10.1016/S1350-4487(03)00053-2
67. Pirazzoli, P. A. *World atlas of Holocene Sea-level changes*. Elsevier B.V., 1991,
68. Lambeck, K. Shoreline reconstructions for the Persian Gulf since the last glacial maximum. *Earth Planet. Sci. Lett.* **1996**, *142*, 43–57 doi:10.1016/0012-821X(96)00069-6
69. Hibbert, F. D., Williams, F. H., Fallon, S. J., & Rohling, E. J. A database of biological and geomorphological sea-level markers from the Last Glacial Maximum to present. *Sci. Data* **2018**, *5*, 1–25 doi:10.1038/sdata.2018.88
70. Rovere, A., Raymo, M. E., Vacchi, M., Lorscheid, T., Stocchi, P., Gómez-Pujol, L., Harris, D. L., Casella, E., O'Leary, M. J., & Hearty, P. J. The analysis of Last Interglacial (MIS 5e) relative sea-level indicators: Reconstructing sea-level in a warmer world. *Earth-Science Rev.* **2016**, *159*, 404–427 doi:10.1016/j.earscirev.2016.06.006
71. Lajoie, K. R. Coastal Tectonics. in *Active Tectonics: Impact on Society* ed. Wallace, R. Washington DC: National Academy Press, 1986, 95–124
72. Otvos, E. G. Beach ridges — definitions and significance. *Geomorphology* **2000**, *32*, 83–108 doi:10.1016/S0169-555X(99)00075-6
73. Tamura, T. Beach ridges and prograded beach deposits as palaeoenvironment records. *Earth-Science Rev.* **2012**, *114*, 279–297 doi:10.1016/j.earscirev.2012.06.004
74. Pedoja, K., Husson, L., Bezos, A., Pastier, A., Imran, A. M., Arias-Ruiz, C., Sarr, A., Elliot, M., Pons-Branchu, E., Nexer, M., Regard, V., Hafidz, A., Robert, X., Benoit, L., Delcaillau, B., Authemayou, C., Dumoulin, C., & Choblet, G. On the long-lasting sequences of coral reef terraces from SE Sulawesi (Indonesia): Distribution, formation, and global significance. *Quat. Sci. Rev.* **2018**, *188*, 37–57 doi:10.1016/j.quascirev.2018.03.033
75. Bird, E. *Coastal Geomorphology, an introduction*. Wiley, 2000,
76. Ashton, A., Murray, A. B., & Arnault, O. Formation of coastline features by large-scale instabilities induced by high-angle waves. *Nature* **2001**, *414*, 296–300 doi:10.1038/35104541
77. Valvo, L. M., Murray, A. B., & Ashton, A. How does underlying geology affect coastline change ? An initial modeling investigation. *J. Geophys. Res.* **2006**, *111*, doi:10.1029/2005JF000340
78. Limber, P. W., Murray, A. B., Adams, P. N., & Goldstein, E. B. Unraveling the dynamics that scale cross-shore headland relief on rocky coastlines: 1. Model development. *J. Geophys. Res. Earth Surf.* **2014**, *119*, 854–873 doi:10.1002/2013JF002950
79. Schwanghart, W., & Kuhn, N. J. TopoToolbox : A set of Matlab functions for topographic analysis. *Environ. Model. Softw.* **2010**, *25*, 770–781 doi:10.1016/j.envsoft.2009.12.002
80. Schwanghart, W., & Scherler, D. Short Communication : TopoToolbox 2 – MATLAB-based software for topographic analysis and modeling in Earth surface sciences. *Earth Surf. Dyn.* **2014**, *2*, 1–7 doi:10.5194/esurf-2-1-2014
81. Limber, P. W., & Murray, A. B. Unraveling the dynamics that scale cross-shore headland relief on rocky coastlines: 2. Model predictions and initial tests. *J. Geophys. Res. Earth Surf.* **2014**, *119*, 874–891 doi:10.1002/2013JF002978
82. Hurst, M. D., Barkwith, A., Ellis, M. A., Thomas, C. W., & Murray, A. B. Exploring the sensitivities of crenulate bay shorelines to wave climates using a new vector-based one-line model. *J. Geophys. Res. Earth Surf.* **2015**, 2586–2608 doi:10.1002/2015JF003704.We
83. Yasso, W. E. Plan Geometry of Headland-Bay Beaches. *J. Geol.* **1965**, *73*, 702–714 doi:10.1086/627111
84. Axe, P., Ilic, S., & Chadwick, A. Evaluation of beach modelling techniques behind detached breakwaters. in *Coastal Engineering Proceedings* 1996, *25*, 2036–2049 doi:10.1061/9780784402429.158
85. Schneider, B. Tsunami and storm sediments in Oman : Characterizing extreme wave deposits using terrestrial laser scanning. *J. Coast. Conserv.* **2018**, doi:10.1007/s11852-018-0663-4

86. Plafker, G. Tectonics of the March 27, 1964 Alaska Earthquake. in *The Alaska Earthquake, March 27, 1964, Regional Effects* U.S. Government Printing Office, 1966, 74 doi:10.3133/pp543
87. Plafker, G., & Savage, J. C. Mechanism of the Chilean Earthquakes of May 21 and 22, 1960. *Geol. Soc. Am. Bull.* **1970**, *81*, 1001–1030 doi:10.1130/0016-7606(1970)81[1001:MOTCEO]2.0.CO;2
88. Sato, T., & Matsu'ura, M. Cyclic crustal movement, steady uplift of marine terraces, and evolution of the island arc-trench system in southwest Japan. *Geophys. J. Int.* **1992**, *111*, 617–629 doi:10.1111/j.1365-246X.1992.tb02116.x
89. Farías, M., Vargas, G., Tassara, A., Carretier, S., Baize, S., Melnick, D., & Bataille, K. Land-Level Changes Produced by the Mw 8.8 2010 Chilean Earthquake. *Science (80-.).* **2010**, *329*, 916 doi:10.1126/science.1192094
90. Simpson, G. Accumulation of permanent deformation during earthquake cycles on reverse faults. *J. Geophys. Res. Solid Earth* **2015**, *120*, 1958–1974 doi:10.1002/2014JB011442
91. Savage, J. C. A Disclocation Model of Strain Accumulation and Release at a Subduction Zone. *J. Geophys. Res.* **1983**, *88*, 4984–4996 doi:10.1029/JB088iB06p04984
92. Ota, Y., & Yamaguchi, M. Holocene coastal uplift in the western Pacific Rim in the context of late Quaternary uplift. *Quat. Int.* **2004**, *120*, 105–117 doi:10.1016/j.quaint.2004.01.010
93. Pedoja, K., Husson, L., Johnson, M. E., Melnick, D., Witt, C., Pochat, S., Nexer, M., Delcaillau, B., Pinegina, T., Poprawski, Y., Authemayou, C., Elliot, M., Regard, V., & Garestier, F. Coastal staircase sequences reflecting sea-level oscillations and tectonic uplift during the Quaternary and Neogene. *Earth-Science Rev.* **2014**, *132*, 13–38 doi:10.1016/j.earscirev.2014.01.007
94. Pinegina, T. K., Bourgeois, J., Kravchunovskaya, E. A., Lander, A. V., Arcos, M. E. M., Pedoja, K., & MacInnes, B. T. A nexus of plate interaction: Vertical deformation of holocene wave-built terraces on the kamchatsky peninsula (kamchatka, russia). *Bull. Geol. Soc. Am.* **2013**, *125*, 1554–1568 doi:10.1130/B30793.1
95. Wesson, R. L., Melnick, D., Cisternas, M., Moreno, M., & Ely, L. L. Vertical deformation through a complete seismic cycle at Isla Santa María , Chile. *Nat. Geosci.* **2015**, *8*, 547–553 doi:10.1038/NGEO2468
96.